Characterizing Spatial Correlation of Blockage Statistics in Urban mmWave Systems

Andrey Samuylov†, Margarita Gapeyenko†, Dmitri Moltchanov†, Mikhail Gerasimenko†,
Sarabjot Singh⋆, Nageen Himayat⋆, Sergey Andreev†, and Yevgeni Koucheryavy†
†W.I.N.T.E.R. Group, Tampere University of Technology, Tampere, Finland
⋆Intel Corporation, Santa Clara, CA, USA.

***Abstract*—Millimeter-wave (mmWave) systems suffer from a significant loss in performance when the line-of-sight (LoS) path between the transmitter and the receiver is obstructed due to blockage caused by humans or other obstacles. However, due to blocker or user motion, the mmWave receiver may transition between the LoS and non-LoS (nLoS) states. Following the recent 3GPP requirements on spatial consistency for channel modeling, this paper aims to analyze the spatial correlation of blockage statistics and characterize their evolution due to user mobility in a static field of blockers in urban mmWave systems. In particular, we derive conditional probabilities of residing in LoS or nLoS state at a given time t_1, provided that a user was in LoS/nLoS state at a prior time t_0. We demonstrate that for realistic values of user speed, the angle of motion, height of transmitter and receiver, as well as the density of blockers, there always is a significant correlation between user channel states at time t_0 and t_1, across the time scales relevant for mmWave resource scheduling. Hence, our model can serve as an important tool for optimizing system performance in the presence of blockage.**

I. Introduction

The need for more capacity at the air interface has led to the standardization of next-generation wireless communications systems (also named "5G") operating in lower parts of the extremely high frequency (EHF) band. Having large bandwidths at their disposal, the so-called *millimeter-wave* (mmWave) technologies are expected to provide the shared rate of around few Gbps enabling throughput-demanding applications and services [1]–[3].

The performance of mmWave systems operating in the EHF band is severely affected by the presence of objects in the wireless channel. As opposed to lower frequencies, mmWaves cannot travel around many objects, thus producing "shaded" locations. Although reflections and diffuse scattering effects in the channel may allow for non-line-of-sight (nLoS) communication, the system performance degrades significantly [4]. As a result, more resources are needed to satisfy user demands when line-of-sight (LoS) is unavailable. In realistic conditions, where a user moves within the coverage area of a mmWave access point, time intervals of "good" and "bad" channel quality alternate affecting the resource allocation.

According to the latest requirements by 3GPP on a new channel model supporting "5G" communication in the range of up to 100 GHz, the small-scale mobility for scenarios such as device-to-device communication should be considered. In addition, the spatial and temporal consistency of the LoS/nLoS states across all user positions is of particular importance for possible massive multiple-input and multiple-output (MIMO) implementation and beam tracking. The channel model in question should be able to capture a smooth change in the LoS/nLoS states as a function of time [5], [6].

The aspects of LoS blockage have been addressed in a number of previous papers [7]–[10]. In [7], the authors studied the problem of LoS blockage, where the buildings block the direct propagation path. The model was introduced for the infinitesimally-small receiver dimension and the blockers occluding the LoS path were distributed uniformly. The said model is similar to the distance-dependent approaches used in 3GPP's urban outdoor micro-cellular model [8]. The comparison between different LoS models for cellular systems, all having various levels of detail, has been completed in [9].

Our previous work in [10] takes into account the key parameters, such as the heights of the transmitter (Tx) and receiver (Rx), the distance between them, the random width and the height of blockers, as well as the human user density across the landscape. These past studies, however, offer a limited insight into blockage modeling. The dependence of the current state of a user on the blockage probability has not been considered and existing results only characterize the unconditional probability for a user to be in LoS/nLoS.

The work on *spatially consistent* large- and small-scale parameters was summarized in [6]. The spatially consistent parameters such as cluster-specific random variables and LoS/nLoS states were generated using the interpolation of independent and identically distributed (i.i.d) random variables. However, this approach did not consider the human body blockage in defining spatially consistent LoS/nLoS states. In [5], such blockage was modeled with rectangular screens dropped onto the simulation map. Further, in [11], the real measurements corroborated an approximation of the attenuation from the human body by the rectangular screen.

However, that model requires tracking of every blocker across the simulation area, which is computationally expensive. In addition, reliance on statistical data does not always allow for setting all of the required parameters flexibly. Finally, in [12], the authors proposed a model for the temporal correlation of interference in a mobile network with a certain density of users. It was demonstrated that correlated propagation states among users significantly impact the temporal interference statistics. However, such analysis did not consider the specifics of human blockage, but only the mean number of obstacles.

In this paper, against the above background, we outline a novel model for the *mobility of Rx* associated with a mmWave access point in the static field of blockers. The proposed model allows considering the *spatial consistency* of the user's states (LoS/nLoS) across different positions. Our analytical framework is able to assess the current state of a user as well as predict the future state evolution after n transmission time intervals (TTIs). The trajectory of Rx is assumed to be a segment of a line with the known angle of motion, velocity, and initial position.

Our results demonstrate that (i) when the time interval between the states of interest is large, there is no dependence on the states of a user, (ii) at *TTI timescales*, there is *high dependence* between the states of the user, and (iii) the dependence between the current and future states of a user decays almost linearly. Our proposed model allows identifying the *dependence time* as well as characterize the *transition probability* between LoS and nLoS conditions in a specified amount of time.

II. Spatial System Model

Consider the scenario illustrated in Fig. 1. The Tx and Rx are located at heights h_T and h_R, respectively. The Rx is moving along a line with the speed of V and the base of Rx is at the distance r_0 from the base of Tx at time t_0. Humans, as potential blockers, are distributed over the landscape and modeled as cylinders [13] with the random height H and the constant base diameter d_m. We assume that the mixture of users' heights can be closely approximated by a Normal distribution $H \sim N(\mu_H, \sigma_H)$ [14]. The centers of cylinder bases are assumed to follow a Poisson point process (PPP) on a plane with the intensity of λ. The size of Rx is assumed to be infinitesimally-small.

Further, Fig. 2 demonstrates the top-view geometric interpretation of the considered scenario. At time t_0, Rx is at the distance r_0 from Tx. As Rx moves at the constant speed V, it travels the distance of $d_0 = (t_1 - t_0)V$ during the time interval $t_1 - t_0$. The angle α denotes the direction of travel. Specifically, α is the angle between the segment of line connecting Tx and Rx at time t_0 and the segment connecting Rx at time t_0 and t_1. Neither velocity nor angle α change during the considered time interval. At the time instant t_1, Rx is at the distance r_1 from Tx. The metrics of interest are the conditional probabilities of LoS/nLoS at time t_1 given that at time t_0 there is LoS/nLoS between Tx and Rx. In what follows, we first obtain the unconditional LoS/nLoS probabilities and then proceed with deriving the conditional ones.

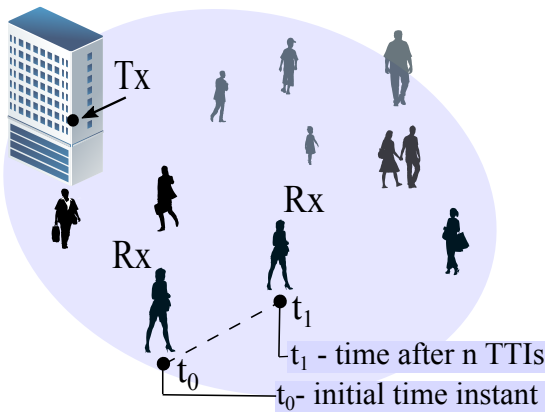

Fig. 1. The considered scenario for our analytical modeling.

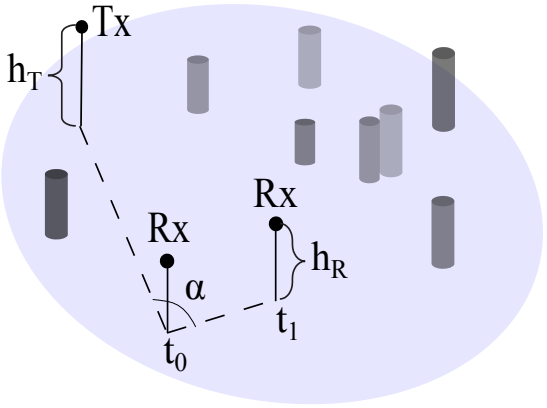

Fig. 2. The geometry of the considered scenario.

III. Conditional LoS/nLoS Probabilities

In this section, we characterize the short-timescale behavior of a mobile user under the assumption that all the possible blockers are stationary. Our aim is to determine the dependence between the LoS and nLoS states at time instants t_0 and t_1 for the timescales relevant for mmWave resource scheduling, as it will be shown in Section IV.

A. LoS/nLoS Probabilities

Before deriving the conditional LoS/nLoS probabilities, we briefly remind the probability of LoS/nLoS at an arbitrary time instant t, when Rx is at a certain distance r from Tx. The probability of LoS is provided in [10] in the form of

$$\mathbb{P}_{\text{LoS}} = p_0 + \sum_{i=1}^{\infty} p_i \prod_{k=1}^{i} \int_0^r f_R(x) \times \\ \times F_H\left(\frac{h_T r - (h_T - h_R)x}{r}\right) dx, \quad (1)$$

where $p_i = (\lambda d_m r)^i e^{-\lambda d_m r}/i!$, $i = 0, 1, \ldots$ are the Poisson probabilities of having i blockers in the rectangle of area $d_m r$ illustrated in Fig. 4, $f_R(x)$ is the probability density function (pdf) of a Uniform distribution from 0 to r, and $F_H(y)$ is the Cumulative Distribution Function (CDF) of the blocker's height.

The above probability of LoS can be given in terms of void probability for the non-homogeneous PPP:

$$\mathbb{P}_{\text{LoS}} = \exp\left(\lambda d_m \times \right. \\ \left. \times \int_0^r F_H\left(\frac{h_T r - (h_T - h_R)x}{r}\right) - 1 \; dx\right). \quad (2)$$

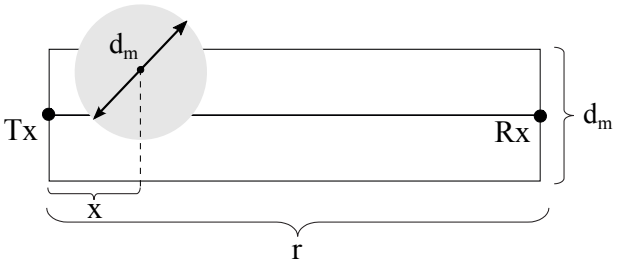

Fig. 3. Top view of the blocking area.

The formulations in (1) and (2) are further employed for the derivation of conditional LoS/nLoS probabilities.

B. Proposed Methodology

Consider Fig. 4 illustrating the top-view of the user movement. At the initial time instant t_0, Tx and Rx are assumed to be located at P and O, respectively. During the time interval $[t_0, t_1]$, Rx moves from point O to point M. We are now interested in the conditional probabilities of user being in LoS/nLoS in the destination point M at the time instant t_1 given that it was in LoS or nLoS at time t_0. These probabilities can be organized into a matrix $\mathbf{P}$ of the following form

$$\mathbf{P} = \begin{pmatrix} p_{00} & p_{01} \\ p_{10} & p_{11} \end{pmatrix}, \tag{3}$$

where states 0 and 1 correspond to LoS and nLoS, respectively, p_{ij} is the conditional probability of a user being in state i at the time instant t_0 and in state j at the time instant t_1. The matrix $\mathbf{P}$ is a function of the following variables:

- r_0: distance from Rx to Tx at time t_0,
- V: velocity of the user,
- $t_1 - t_0$: time interval of user movement,
- α: angle of movement,
- λ: density of blockers.

It is important to note that

$$p_{00} = 1 - p_{01}, \quad p_{10} = 1 - p_{11}. \tag{4}$$

Moreover, note that the following holds

$$\mathbb{P}_{\mathrm{LoS,M}} = p_{00}\mathbb{P}_{\mathrm{LoS,O}} + p_{10}\mathbb{P}_{\mathrm{nLoS,O}}, \tag{5}$$

where $\mathbb{P}_{\mathrm{LoS,M}}$, $\mathbb{P}_{\mathrm{LoS,O}}$, and $\mathbb{P}_{\mathrm{nLoS,O}}$ are derived using (1) or (2) provided in Section III-A. Therefore, in order to parametrize (3), it suffices to establish p_{00}.

To illustrate the proposed methodology, consider two rectangles related to the area affecting the LoS path, when Rx is at the point O at time t_0 and at the point M at time t_1 as illustrated in Fig. 4. The width of these rectangles equals the diameter of a blocker d_m and their lengths are the distances r_0 and r_1 between the bases of Tx and Rx at time t_0 and t_1, respectively. Observe that the intersection of two rectangles graphically illustrates the dependence between the states at time t_0 and t_1. As one may further notice in Fig. 4, the intersection of these areas is larger or smaller depending on t_1, α, and V. The proposed approach is based on the extension of the method described in Section III-A for a point stationary Rx. To capture the dependence between the state of the user at t_0 and t_1, we have to account for the common zone, where possible blockers may impact the states at both Rx locations.

Our scenario in question can be decomposed into several zones having different shapes. We partition it into four major zones having various impacts on the conditional probabilities of interest, as shown in Fig. 4. These are:

- **Zone 1**, $NN'LR$, includes the square area around the Tx. Since the height of Tx, h_T, is assumed to exceed the maximum height of humans, the impact of this zone is negligible.
- **Zone 2**, $ANSKD$, corresponds to the initial LoS path and will affect the conditional probability only when Rx is in the nLoS state at the time instant t_0.
- **Zone 3**, $IKEH$, only affects the LoS path to the destination and is the major factor contributing to the conditional probabilities of interest for longer movement distances.
- **Zone 4**, SRK, is the intersection of the two areas affecting both LoS paths simultaneously. This zone is a major contributor to the dependence between the states of the user at time instants t_0 and t_1.

We further split zone 4 into two smaller zones, $4a$ and $4b$, along the line of intersection between the two planes corresponding to the two LoS paths, as shown in Fig. 5. Zone $4a$ is a part of zone 4, where the LoS path to the destination is lower than the LoS path to the origin, i.e., a single blocker can be high enough to block the LoS at t_1, while it might be too low to block it at t_0. In zone $4b$, the situation is reverse, i.e., the LoS path at t_1 is higher than the LoS path at t_0.

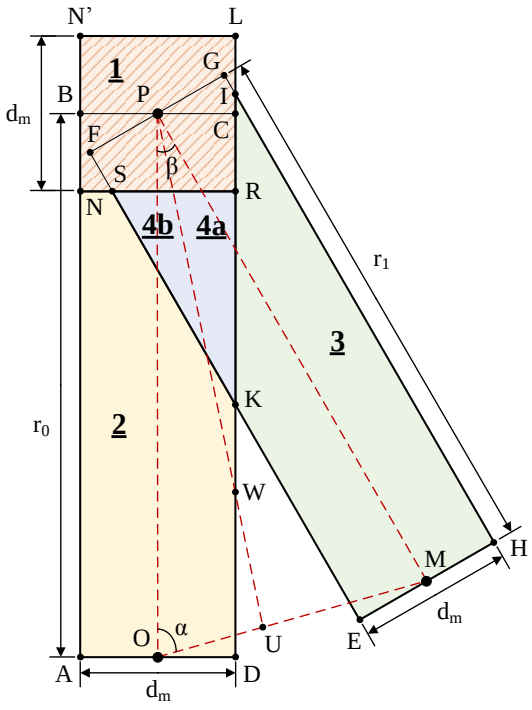

Fig. 4. 2D view of the user movement.

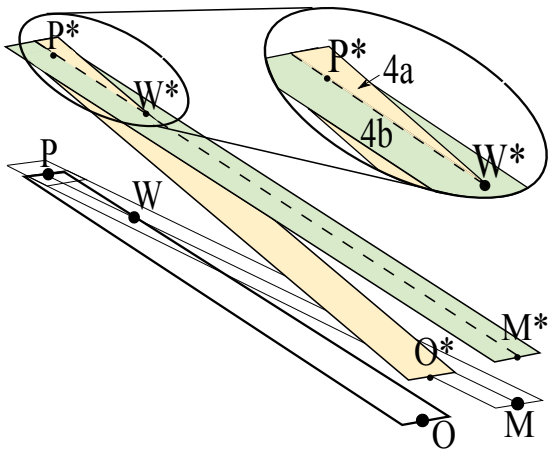

Fig. 5. 3D view of the user movement.

Even though our above decomposition is general and holds for any choice of input parameters, for some particular cases certain zones may become irrelevant. The latter, however, does not affect the generality of our derived results, as it is shown further, since the corresponding probabilities can be substituted by 1 or 0 wherever appropriate. All these more detailed cases are covered at length in our technical report [15]. Once the appropriate zones are identified, we derive the conditional probabilities of LoS/nLoS by following the approach developed in Section III-A.

C. Probabilities p_{00} and p_{01}

The conditional probability p_{00} can be written as

$$p_{00} = \mathbb{P}\left[\text{LoS at M}|\text{LoS at O}\right] = \\ = \frac{\mathbb{P}\left[\text{LoS at M} \cap \text{LoS at O}\right]}{\mathbb{P}\left[\text{LoS at O}\right]}. \tag{6}$$

According to the methodology described earlier, we now subdivide the events associated with this conditional probability into smaller events. Let $\widetilde{L}_z$ and L_z be the events when LoS is not blocked in zone z for points O and M, respectively. This may happen when there are no blockers in this zone and/or when all of the blockers are lower than the LoS path. Observe that the event [LoS at M] is equivalent to the event $L_3 \cap L_{4a} \cap L_{4b}$, while the event [LoS at O] is equivalent to the event $\widetilde{L}_2 \cap \widetilde{L}_{4a} \cap \widetilde{L}_{4b}$. Here, $\widetilde{L}_{4a} \cap L_{4a} = L_{4a}$, which directly follows from the geometry of the considered scenario. Note that the zone $4a$ belongs to both planes, one of them being higher than another. When a blocker does not intersect the lower plane of the zone $4a$, the plane (FGH) in Fig. 5, it does not intersect the upper plane either. The same applies to $\widetilde{L}_{4b} \cap L_{4b} = \widetilde{L}_{4b}$. Note also that $\widetilde{L}_z$ is only dependent on L_z. Hence, (6) can be written as

$$p_{00} = \frac{\mathbb{P}\left[L_3 \cap L_{4a} \cap L_{4b} \cap \widetilde{L}_2 \cap \widetilde{L}_{4a} \cap \widetilde{L}_{4b}\right]}{\mathbb{P}\left[\widetilde{L}_2 \cap \widetilde{L}_{4a} \cap \widetilde{L}_{4b}\right]}. \tag{7}$$

Simplifying, we obtain

$$p_{00} = \frac{\mathbb{P}\left[L_3 \cap L_{4a}\right]}{\mathbb{P}\left[\widetilde{L}_{4a}\right]}. \tag{8}$$

The conditional probability p_{00} is thus given by

$$p_{00} = \frac{\mathbb{P}_{nb3}\mathbb{P}_{nb4a}}{\widetilde{\mathbb{P}}_{nb4a}}, \tag{9}$$

where nb stands for "no blockers" and $\mathbb{P}_{nb\ \mathrm{z}}$ is the probability of the event L_z.

Recalling the methodology for deriving the LoS probability in Section III-A, we apply similar principles to obtain $\mathbb{P}_{nb\ \mathrm{z}}$, where z is the number of the considered zone. We thus have

$$\mathbb{P}_{nb\ \mathrm{z}} = f_P(0, \lambda\ S_z) + \sum_{i=1}^{\infty} f_P(i, \lambda\ S_z) \times \\ \times \prod_{k=1}^{i} \frac{1}{S_z} \left(\int_{x_1}^{x_2} \int_{y_1}^{y_2} F_H\left(\frac{gy - fx - e}{h}\right) dy\ dx + \cdots \right. \\ \left. + \int_{x_j}^{x_{j+1}} \int_{y_j}^{y_{j+1}} F_H\left(\frac{gy - fx - e}{h}\right) dy\ dx \right), \tag{10}$$

where all the auxiliary parameters are defined in [15], $f_P(i, \lambda)$ is the probability of having exactly i blockers in the area of interest for a given density of blockers λ, S_z is the area under the required zone needed to specify the pdf for a point distributed uniformly in the zone, and $F_H\left(\frac{gy-fx-e}{h}\right)$ is the probability that a blocker located at the coordinates x, y is lower than the LoS. Variables $x_j, x_{j+1}, y_j, y_{j+1}$ represent the boundaries x and y of the considered area.

As the sum of integrals in (10) is independent of k, we can substitute it by an auxiliary variable I. Additionally, substituting the Poisson probabilities into (10), we establish

$$\mathbb{P}_{nb\ \mathrm{z}} = e^{-\lambda S_z} + \sum_{i=1}^{\infty} \frac{(\lambda S_z)^i e^{-\lambda S_z}}{i!} \left(\frac{I}{S_z}\right)^i. \tag{11}$$

As one may observe, the first two summands in (11) are the Maclaurin series expansion of an exponential function, and thus (11) is simplified to

$$\mathbb{P}_{nb\ \mathrm{z}} = e^{\lambda(I - S_z)}. \tag{12}$$

Expanding the auxiliary variable I, we produce

$$\mathbb{P}_{nb\ \mathrm{z}} = \exp\left(\lambda \times \right. \\ \left. \times \int_{x_1}^{x_2} \int_{y_1}^{y_2} \left(F_H\left(\frac{gy - fx - e}{h}\right) - 1 \right) dy\ dx \right) \times \cdots \\ \times \exp\left(\lambda \times \right. \\ \left. \times \int_{x_j}^{x_{j+1}} \int_{y_j}^{y_{j+1}} \left(F_H\left(\frac{gy - fx - e}{h}\right) - 1 \right) dy\ dx \right). \tag{13}$$

Probabilities $\mathbb{P}_{nb\ \mathrm{z}}$ are calculated using (10), while all the necessary integration limits are provided in [15]. Observe that $\widetilde{\mathbb{P}}_{nb\ \mathrm{z}}$ denote the probabilities of having no blockers affecting

the LoS in the corresponding zones for point O. That is, the individual blockers must be lower than the plane (ABC) in Fig. 5. Hence, the probabilities $\widetilde{\mathbb{P}}_{nb\ z}$ are obtained similarly to $\mathbb{P}_{nb\ z}$ and have the following form

$$\widetilde{\mathbb{P}}_{nb\ z} = \exp\Bigg(\lambda\times \times \int_{x_1}^{x_2}\int_{y_1}^{y_2}\left(F_H\left(\frac{by-ax-d}{c}\right)-1\right)dy\ dx\Bigg)\times\cdots \times \exp\Bigg(\lambda\times \times \int_{x_j}^{x_{j+1}}\int_{y_j}^{y_{j+1}}\left(F_H\left(\frac{by-ax-d}{c}\right)-1\right)dy\ dx\Bigg). \quad (14)$$

D. Probabilities p_{10} and p_{11}

The probability p_{10} could be expressed from (5) as

$$p_{10} = \frac{\mathbb{P}_{\mathrm{LoS,M}} - p_{00}\mathbb{P}_{\mathrm{LoS,O}}}{\mathbb{P}_{\mathrm{nLoS,O}}} = \frac{\mathbb{P}_{\mathrm{LoS,M}} - p_{00}\mathbb{P}_{\mathrm{LoS,O}}}{1-\mathbb{P}_{\mathrm{LoS,O}}}, \quad (15)$$

where $\mathbb{P}_{\mathrm{LoS,M}}$ and $\mathbb{P}_{\mathrm{LoS,O}}$ are derived from (2) in Section III-A as

$$\mathbb{P}_{\mathrm{LoS,M}} = \exp\left(\lambda d_m\times \times \int_0^{r_1}\left(F_H\left(\frac{h_T r_1-(h_T-h_R)x}{r_1}\right)-1\right)dx\right)$$
$$\mathbb{P}_{\mathrm{LoS,O}} = \exp\left(\lambda d_m\times \times \int_0^{r_0}\left(F_H\left(\frac{h_T r_0-(h_T-h_R)x}{r_0}\right)-1\right)dx\right). \quad (16)$$

Finally, the matrix **P** containing the conditional probabilities could be parametrized by (4), (9), and (15).

IV. Numerical Results

To assess the accuracy of the proposed model, we first compare our results against those obtained with system-level simulations. The main difference between the simulation and the analysis is in the presence of position estimation error within the simulated data. According to [16], we model the position estimation error as a constant offset in the initial Rx location. For simplicity, we do not account for velocity and direction errors assuming that their effects may be reduced significantly by using accelerometers and other sensors at Rx. However, location and trajectory prediction could still be problematic, since the estimation error may be up to several meters depending on the type of device and navigation system [16]. In this paper, we consider two options: 1 m and 3 m error, which correspond to the minimum and the average error for the Assisted GPS device.

As we observe in Fig. 6, even when the position estimation error is accounted for, there is an acceptable agreement between the analysis and simulation data. Hence, in what follows we assess the effects of user mobility by relying on our proposed analytical model. Further, Fig. 6 illustrates the conditional and unconditional LoS probabilities for the baseline parameters listed in Table I as a function of t_1. Analyzing the underlying structure of the studied variables, one may observe a clear dependence between the states of a user over the time scales of interest. Recalling that the TTI interval in mmWave systems is around 100 μs [3], the scheduling decisions should be heavily affected by the user movement. As the time interval of interest extends, this dependence vanishes and the conditional probabilities converge to their unconditional counterparts.

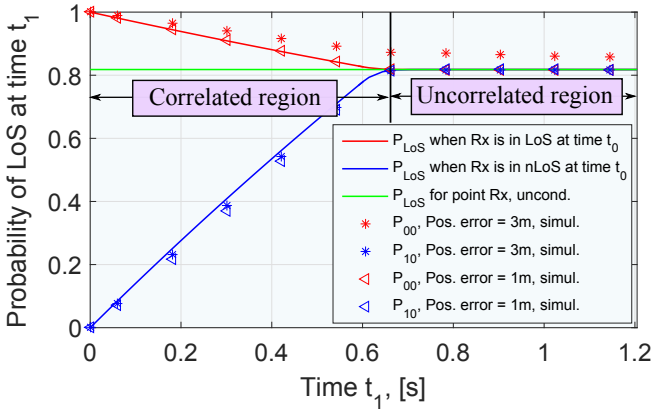

Fig. 6. Comparison of analysis and simulation results.

To gain insights into the qualitative behavior of the studied variables, the *conditional LoS probabilities* as functions of t_1, r_0, V, h_R, h_T, λ, and α are shown in Fig. 7. The variations in distance r_0 affect the conditional probabilities. At the same time, user velocity does not alter the probability of LoS, but produces a strong impact on the *correlation time*. Indeed, for a user moving at 5 km/h this time is almost twice shorter compared to that for a user moving at 3 km/h. The effect of Rx height is more curious since h_R affects not only unconditional, but also conditional LoS probabilities. However, due to a limited realistic range of h_R, this parameter does not produce a significant impact in practice.

The effect of h_T is similar to that of h_R. The major difference though is in that the feasible range of h_T is expected to be much broader compared to that of h_R. It is also important to note that this parameter impacts the behavior of

TABLE I
Baseline System Parameters

Parameter	Value
Height of Tx, h_T	4 m
Height of Rx, h_R	1.5 m
Initial distance between the bases of Tx and Rx, r_0	50 m
Height of a blocker, $N(\mu_H, \sigma_H)$	$N(1.7\text{ m}, 0.1\text{ m})$
Diameter of a blocker, d_m	0.5 m
Intensity of blockers, λ	0.1 blockers/m^2
Speed of Rx, V	3 km/h
Angle of motion, α	$\pi/2$

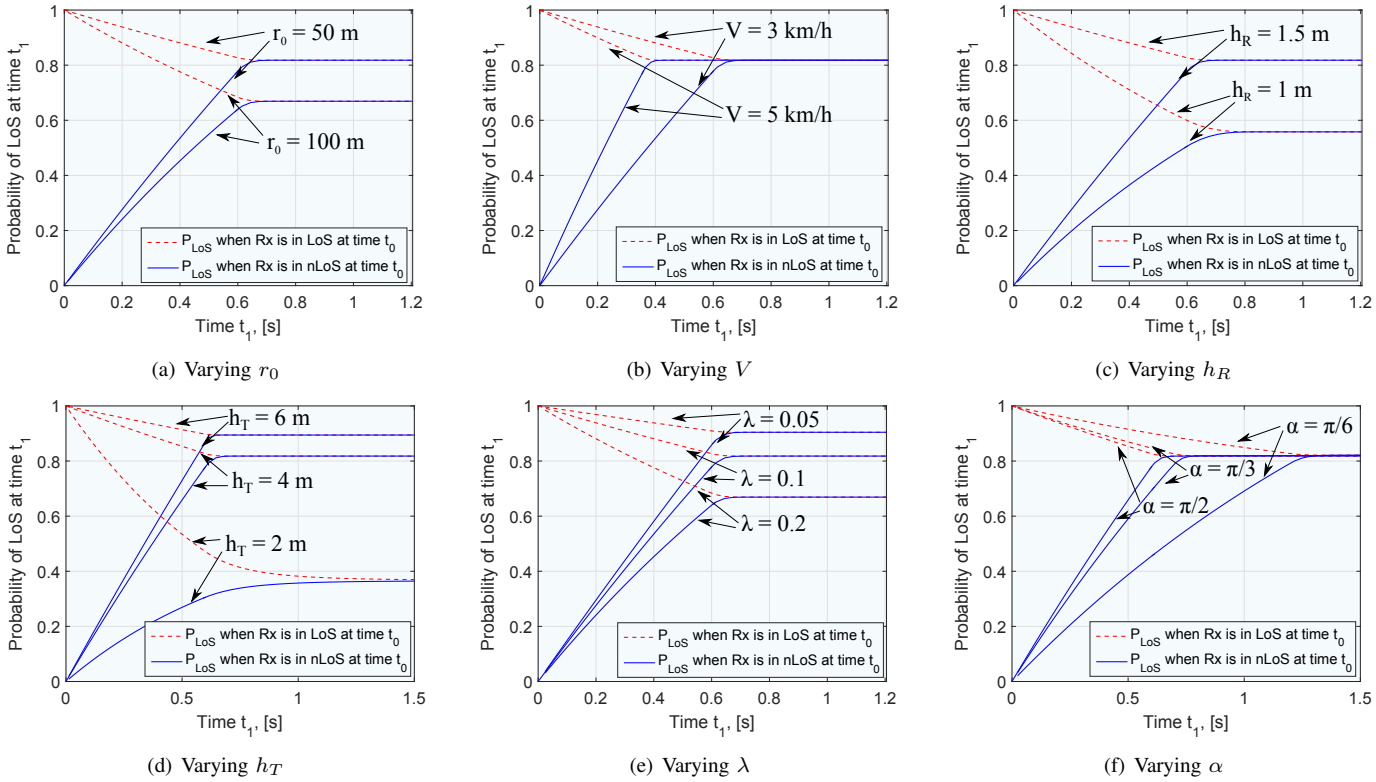

(a) Varying r_0 (b) Varying V (c) Varying h_R

(d) Varying h_T (e) Varying λ (f) Varying α

Fig. 7. Conditional and unconditional LoS probabilities as functions of input parameters.

our result qualitatively, that is, changes its structure. Indeed, for small values of h_T there is an exponentially decaying loss of memory between the states. As h_T increases, the behavior becomes close to linear. By varying the intensity of blockers, λ, one may notice that higher intensity leads to a higher probability of blockage, as well as brings changes to the temporal behavior of the conditional probabilities. Finally, different angles of motion α have a profound effect on the values of LoS probability. As the angle α decreases, the correlation between the states grows, thus leading to a longer fraction of time when the state t_1 depends on the state t_0.

Let us now study the behavior of the *correlation time* between the states of a user, which we define as a time interval until the conditional and the unconditional probabilities converge. To this end, Fig. 8 reports this variable as a function of the input parameters and we learn that the initial position does not affect the correlation time significantly. As it could be noticed in Fig. 8(b), the actual velocity impacts the correlation time strongly: as the former increases the latter decreases.

For h_R and h_T, the correlation time has a lower bound on this value. While there is no impact on the height of Rx, deploying the mmWave access points higher than at 4 m not only decreases the unconditional blocking probability but also ensures much shorter correlation time, thus giving more flexibility for the potential resource scheduling algorithm. Moreover, the correlation time does not change significantly as the height of Tx becomes greater than 4 m.

The effects of the density of blockers on the correlation time are of particular importance. Indeed, if there would be a significant dependence of this value not only on the access point and user related parameters, but also on the environment of interest, then for efficient resource allocation a mmWave access point would need to know the density of users. However, the correlation time does not appear to be considerably dependent on the density of users, as indicated in Fig. 8(e).

The dependence on the moving angle α is more intricate. When a user moves along a line that is close to 0 or π, the correlation time is extremely long. The reason is that the probability of leaving the previous state is very low. For values in between 0.5 rad and 2.5 rad, the correlation time is almost constant. Note also that changing the Tx height does not impact the correlation time substantially for a given motion angle.

V. Conclusions

Motivated by the 3GPP requirements regarding the spatially consistent channel model for the next-generation wireless communications systems, we analyzed the conditional probabilities of LoS blockage as functions of various system parameters, including the speed of a user, its motion angle, the heights of transmitter and receiver, as well as the density of blockers. Our main conclusion is that for realistic system parameters and timescales typical for mmWave resource scheduling, there always is a considerable dependence between the previous state of the user and its current state.

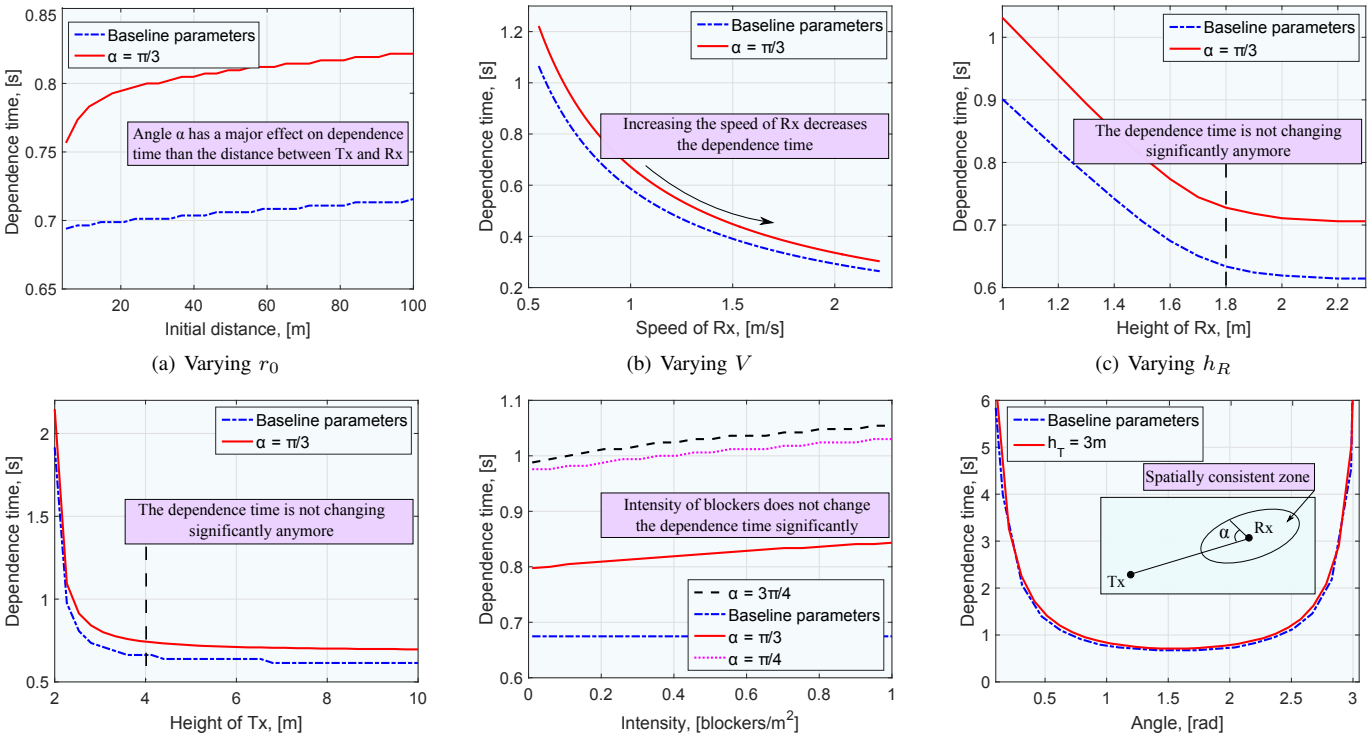

(a) Varying r_0 (b) Varying V (c) Varying h_R

(d) Varying h_T (e) Varying λ (f) Varying α

Fig. 8. Dependence time as a function of input parameters.

Our proposed model allows to accurately account for said dependence. In addition to the conditional LoS/nLoS probabilities, we also introduced and analyzed in detail the correlation time between the states of a user. An important outcome here is that the position of Rx at time instants t_0 and t_1 affects the correlation time between the states of a user. The latter implies that for efficient resource allocation at the air interface, the mmWave access points need to consider the current state of Rx.

Acknowledgment

This work is supported by Intel Corporation as well as by the Academy of Finland.

References

[1] J. G. Andrews, S. Buzzi, C. Wan, S. V. Hanly, A. Lozano, A. C. K. Soong, and J. C. Zhang, "What will 5G be?," *IEEE Journal on Selected Areas in Communications*, vol. 32, pp. 1065–1082, June 2014.

[2] T. S. Rappaport, S. Sun, R. Mayzus, H. Zhao, Y. Azar, K. Wang, G. N. Wong, J. K. Schulz, M. K. Samimi, and F. Gutierrez Jr., "Millimeter Wave Mobile Communications for 5G Cellular: It Will Work!," *IEEE Access*, vol. 1, pp. 335–349, May 2013.

[3] A. Ghosh, T. A. Thomas, M. C. Cudak, R. Ratasuk, P. Moorut, F. W. Vook, T. S. Rappaport, G. R. MacCartney, S. Sun, and S. Nie, "Millimeter-wave enhanced local area systems: a high-data-rate approach for future wireless networks," *IEEE Journal on Selected Areas in Communications*, vol. 32, pp. 1152–1163, June 2014.

[4] M. R. Akdeniz, Y. Liu, M. K. Samimi, S. Sun, S. Rangan, T. S. Rappaport, and E. Erkip, "Millimeter wave channel modeling and cellular capacity evaluation," *IEEE Journal on Selected Areas in Communications*, vol. 32, pp. 1164–1179, June 2014.

[5] "Channel model for frequency spectrum above 6 GHz (Release 14)," *3GPP TR 38.900 V2.0.0*, June 2016.

[6] A. Ghosh *et al.*, "5G channel model for bands up to 100 GHz," 5GCM white paper, 2015.

[7] T. Bai, R. Vaze, and R. W. Heath Jr., "Using random shape theory to model blockage in random cellular networks," in *Proc. of International Conference on Signal Processing and Communications (SPCOM)*, July 2012.

[8] "Evolved Universal Terrestrial Radio Access (E-UTRA); Further advancements for E-UTRA physical layer aspects (Release 9)," *3GPP TR 36.814 V9.0.0*, March 2010.

[9] M. N. Kulkarni, S. Singh, and J. G. Andrews, "Coverage and rate trends in dense urban mmWave cellular networks," in *Proc. of IEEE Global Communications Conference (GLOBECOM)*, December 2014.

[10] M. Gapeyenko, A. Samuylov, M. Gerasimenko, D. Moltchanov, S. Singh, E. Aryafar, S. Yeh, N. Himayat, S. Andreev, and Y. Koucheryavy, "Analysis of human-body blockage in urban millimeter-wave cellular communications," in *Proc. of IEEE International Conference on Communications (ICC)*, May 2016.

[11] G. R. MacCartney Jr., S. Deng, S. Sun, and T. S. Rappaport, "Millimeter-wave human blockage at 73 GHz with a simple double knife-edge diffraction model and extension for directional antennas," in *Proc. of IEEE Vehicular Technology Conference (VTC Fall)*, September 2016.

[12] K. Koufos and C. P. Dettmann, "Temporal correlation of interference in bounded mobile ad hoc networks with blockage," *IEEE Communications Letters*, August 2016.

[13] M. Jacob, S. Priebe, T. Kurner, M. Peter, M. Wisotzki, R. Felbecker, and W. Keusgen, "Fundamental analyses of 60 GHz human blockage," in *Proc. of European Conference on Antennas and Propagation (EuCAP)*, April 2013.

[14] C. L. Ogden, C. D. Fryar, M. D. Carroll, and K. M. Flegal, "Mean body weight, height, and body mass index, United States 1960–2002," *Centers for Disease control and prevention*, October 2004.

[15] A. Samuylov *et al.*, "Characterizing spatial correlation of blockage statistics," technical report available at: http://winter-group.net/downloads/mmWave_blockage_report.pdf, Tampere University of Technology, 2016.

[16] P. A. Zandbergen and S. J. Barbeau, "Positional accuracy of Assisted GPS data from high-sensitivity GPS-enabled mobile phones," *The Journal of Navigation*, vol. 64, pp. 381–399, July 2011.